UV−Visible Absorption Spectra of [Ru(E)(E′)(CO)$_2$(iPr-DAB)] (E = E′ = $SnPh_3$ or Cl; E = $SnPh_3$ or Cl, E′ = CH_3; iPr-DAB = *N*,*N*′-Di-isopropyl-1,4-diaza-1,3-butadiene): Combination of CASSCF/CASPT2 and TD-DFT Calculations

Mohamed Turki,[†] Chantal Daniel,*[,†] Stanislav Záliš,*[,‡] Antonín Vlček, Jr.,*[,‡,§] Joris van Slageren,[||] and Derk J. Stufkens*[,||]

Contribution from the Laboratoire de Chimie Quantique UMR 7551 CNRS / Université Louis Pasteur Institut LeBel, 4 Rue Blaise Pascal, F- 67 000 Strasbourg, France, the J. Heyrovský Institute of Physical Chemistry, Academy of Sciences of the Czech Republic, Dolejškova 3, CZ-182 23 Prague 8, Czech Republic, the Department of Chemistry, Queen Mary and Westfield College (University of London), Mile End Road, London E1 4NS, U.K., and the Institute of Molecular Chemistry, Universiteit van Amsterdam, Nieuwe Achtergracht 166, NL-1018 WV Amsterdam, The Netherlands

Received March 26, 2001. Revised Manuscript Received July 9, 2001

Abstract: The UV−visible absorption spectra of [Ru(E)(E′)(CO)$_2$(iPr-DAB)] (E = E′ = $SnPh_3$ or Cl; E = $SnPh_3$ or Cl, E′ = CH_3; iPr-DAB = *N*,*N*′-di-isopropyl-1,4-diaza-1,3-butadiene) are investigated using CASSCF/CASPT2 and TD-DFT calculations on model complexes [Ru(E)(E′)(CO)$_2$(Me-DAB)] (E = E′ = SnH_3 or Cl; E = SnH_3 or Cl, E′ = CH_3; Me-DAB = *N*,*N*′-dimethyl-1,4-diaza-1,3-butadiene). The calculated transition energies and oscillator strengths allow an unambiguous assignment of the spectra of the nonhalide complexes [Ru($SnPh_3$)$_2$(CO)$_2$(iPr-DAB)] and [Ru($SnPh_3$)(Me)(CO)$_2$(iPr-DAB)]. The agreement between the CASSCF/CASPT2 and TD-DFT approaches is remarkably good in the case of these nonhalide complexes. The lowest-energy part of the spectrum (visible absorption) originates in electronic transitions that correspond to excitations from the axial E−Ru−E′ σ_2 orbital into the low-lying π^*_{DAB} orbital (σ-bond-to-ligand charge transfer, SBLCT, transitions), while the absorption between 25 000 and 35 000 cm^{-1} is due to metal-to-ligand charge transfer (MLCT) excitations from the $4d_{Ru}$ orbitals to π^*_{DAB} (MLCT). Above 35 000 cm^{-1}, the transitions mostly correspond to MLCT and SBLCT excitations into π^*_{CO} orbitals. Analysis of the occupied σ orbitals involved in electronic transitions of the nonhalide complexes shows that the Kohn−Sham orbitals are generally more delocalized than their CASSCF/CASPT2 counterparts. The CASSCF/CASPT2 and TD-DFT approaches lead to different descriptions of electronic transitions of the halide complexes [Ru(Cl)$_2$(CO)$_2$(Me-DAB)] and [Ru(Cl)(Me)(CO)$_2$(Me-DAB)]. CASSCF/CASPT2 reproduces well the observed blue-shift of the lowest absorption band on going from the nonhalide to halide complexes. TD-DFT systematically underestimates the transition energies of these complexes, although it reproduces the general spectral features. The CASSCF/CASPT2 and TD-DFT techniques differ significantly in their assessment of the chloride contribution. Thus, CASSCF/CASPT2 assigns the lowest-energy absorption to predominantly Ru → DAB MLCT transitions, while TD-DFT predicts a mixed XLCT/MLCT character, with the XLCT component being predominant. (XLCT stands for halide (X)-to-ligand-charge transfer.) Analysis of Kohn−Sham orbitals shows a very important $3p_{Cl}$ admixture into the high-lying occupied orbitals, in contrast to the CASSCF/CASSPT2 molecular orbitals which are nearly pure $4d_{Ru}$ with the usual contribution of the back-donation to π^*_{CO} orbitals. Further dramatic differences were found between characters of the occupied σ orbitals, as calculated by CASSCF/CASPT2 and DFT. They differ even in their bonding character with respect to the axial E−Ru and Cl−Ru bonds. These differences are attributed to a drawback of the DFT technique with respect to the dynamical correlation effects which become very important in complexes with a polar Ru−Cl bond. Similar differences in the CASSCF/CASPT2 and TD-DFT descriptions of the lowest allowed transition of [Ru(Cl)$_2$(CO)$_2$(Me-DAB)] and [Ru(Cl)(Me)(CO)$_2$(Me-DAB)] were found by comparing the changes of Mulliken population upon excitation. This comparison also reveals that CASSCF/CASPT2 generally predicts smaller electron density redistribution upon excitation than TD-DFT, despite the more localized character of CASSCF/CASPT2 molecular orbitals.

Introduction

Transition metal carbonyl−diimine complexes [Ru(E)(E′)(CO)$_2$(α-diimine)] (E, E′ = halide, alkyl, benzyl, metal-fragment; α-diimine = derivatives of 1,4-diaza-1,3-butadiene or 2,2′-bipyridine), Figure 1, have very unconventional photochemical, photophysical, and electrochemical properties.[1−16] In

[†] CNRS / Université Louis Pasteur Institut LeBel.
[‡] Academy of Sciences of the Czech Republic.
[§] Queen Mary and Westfield College (University of London).
[||] Universiteit van Amsterdam.

(1) Nieuwenhuis, H. A.; Stufkens, D. J.; Oskam, A. *Inorg. Chem.* **1994**, *33*, 3212.
(2) Nieuwenhuis, H. A.; Stufkens, D. J.; Oskam, A.; Vlček, A., Jr. *Inorg. Chem.* **1995**, *34*, 3879.

10.1021/ja010782b CCC: $20.00 © 2001 American Chemical Society
Published on Web 10/30/2001

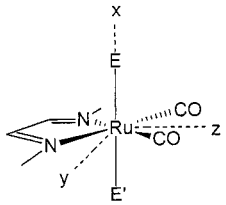

Figure 1. Idealized structure of the complexes $[Ru(E)(E')(CO)_2(Me\text{-}DAB)]$ and chosen orientation of the axes.

a series of structurally related compounds, or even within the same molecule, we encounter several different types of charge-transfer transitions from the metal, the halide ligand, or even the axial σ bond to the electron accepting α-diimine ligand. Other transitions are directed to the carbonyls. Electron delocalization, charge separation, and their spectroscopic and photochemical consequences are further important issues. These spectroscopic and structural features are a big challenge to the interplay between theory and experiment and have important implications for the spectroscopy and photochemistry of the broad and important class of low-valent metal complexes containing simultaneously electron-accepting ligands and π donors such as halides and/or σ-bonded alkyl or metal-fragment ligands. Moreover, the $[Ru(E)(E')(CO)_2(\alpha\text{-diimine})]$ complexes have themselves great potential as luminophores,[14] photosensitizers, and visible-light photoinitiators of radical reactions.[17] Their photochemistry and photophysics represent a challenge to the understanding of excited states dynamics.[14,18,19]

According to their spectroscopic and photochemical properties, the $[Ru(E)(E')(CO)_2(\alpha\text{-diimine})]$ complexes can be classified into two distinct groups: (i) complexes in which at least one of the E, E′ ligands is a halide and (ii) complexes where E and E′ are either an alkyl group or a metal-fragment, but not a halide. The halide-containing complexes[1−3,13] show a solvatochromic absorption band in the 430−450 nm range. Their resonance Raman spectra are dominated by a strongly enhanced band due to the $\nu_S(CN)$ vibration of the α-diimine ligand. The $\nu_S(CO)$ Raman band is enhanced only weakly or is absent. The halide complexes are photostable. By contrast, the complexes which do not contain a halide ligand are characterized[5,13] by a much stronger band at longer wavelengths, between 510 and 550 nm, which is only weakly solvatochromic. Their resonance Raman spectra show many moderately enhanced bands, indicating that the resonant electronic transition is highly delocalized. Irradiation of these complexes leads to homolysis of a metal−ligand (E′) bond, producing radicals.[6,13,15,17] On the basis of the UV−vis and resonance Raman spectral features and preliminary DFT calculations performed on the model systems $[Ru(E)(E')(CO)_2(H\text{-}DAB)]$ ($E = E' = SnH_3$; $E = SnH_3$ or Cl, $E' = CH_3$), the visible absorption band observed for $[Ru(SnPh_3)_2(CO)_2(iPr\text{-}DAB)]$ and $[Ru(SnPh_3)(Me)(CO)_2(iPr\text{-}DAB)]$ has been attributed[5,13] to the σ-bond-to-ligand charge transfer (SBLCT) electronic transition which corresponds to $\sigma_{E-Ru-E'} \rightarrow \pi^*_{DAB}$ excitation, whereas the lowest band in $[Ru(Cl)(Me)(CO)_2(iPr\text{-}DAB)]$ has been assigned to a mixed metal/halide-to-DAB charge transfer transition, which corresponds mainly to $4d_{Ru}/3p_{Cl} \rightarrow \pi^*_{DAB}$ excitation.[1−3,13] This transition is denoted as XLCT/MLCT, which stands for halide (X)-to-ligand charge transfer/metal-to-ligand charge transfer. However, these early calculations did not reproduce the large red shift of the main visible absorption band observed on going from the halide to the nonhalide complexes, casting some doubt on the overall spectral assignment. Moreover, no attempt was made to assign higher absorption bands occurring in the UV spectral region.

The correct description of electronic transitions in $[Ru(E)(E')(CO)_2(\alpha\text{-diimine})]$ complexes is much needed, not only because of its fundamental importance, but especially to understand the dramatic dependence of the photophysics and photochemistry of these complexes on the ligands E and E′. Therefore, a detailed theoretical investigation of electronic transitions of the model complexes $[Ru(E)(E')(CO)_2(Me\text{-}DAB)]$ ($E = E' = SnH_3$ or Cl; SnH_3 or Cl, $E' = CH_3$) was undertaken, using two different quantum chemical techniques: CASSCF/CASPT2 and TD-DFT. In the CASSCF/CASPT2 method, the dynamical electronic correlation is added as a perturbation on top of a zero-order multiconfigurational wave function. The time-dependent DFT technique, TD-DFT, is a first-principle method for calculating response properties such as transition energies. This theoretical treatment is much superior to the DFT-based ΔSCF technique used previously.[5,13] The iPr-DAB ligand is modeled as Me-DAB instead of as the simpler H-DAB model used before.

This study was carried out with several goals: (i) to make a complete assignment of the UV−vis spectra of $[Ru(E)(E')(CO)_2(R\text{-}DAB)]$ complexes with a special emphasis on the low-energy transitions responsible for the visible absorption, (ii) to establish the differences in the electronic structure and understand the different spectroscopic properties of the halide and nonhalide complexes, and (iii) to compare the CASSCF/CASPT2 and TD-DFT theoretical approaches and their applicability to the assignment of electronic absorption spectra of organometallic compounds. In addition, striking differences between the CASSCF and DFT descriptions of the bonding in the studied molecules at an orbital level have emerged.

Experimental Section

The following complexes were prepared according to the literature procedures: $[Ru(Cl)_2(CO)_2(iPr\text{-}DAB)]$,[20] $[Ru(Cl)(Me)(CO)_2(iPr\text{-}DAB)]$,[1] $[Ru(SnPh_3)(Me)(CO)_2(iPr\text{-}DAB)]$,[7] and $[Ru(SnPh_3)_2(CO)_2(iPr\text{-}DAB)]$.[5] The UV−vis absorption spectra of the complexes dissolved in cyclo-

(3) Nieuwenhuis, H. A.; Stufkens, D. J.; McNicholl, R.-A.; Al-Obaidi, A. H. R.; Coates, C. G.; Bell, S. E. J.; McGarvey, J. J.; Westwell, J.; George, M. W.; Turner, J. J. *J. Am. Chem. Soc.* **1995**, *117*, 5579.
(4) Nieuwenhuis, H. A.; van de Ven, M. C. E.; Stufkens, D. J.; Oskam, A.; Goubitz, K. *Organometallics* **1995**, *14*, 780.
(5) Aarnts, M. P.; Wilms, M. P.; Peelen, K.; Fraanje, J.; Goubitz, K.; Hartl, F.; Stufkens, D. J.; Baerends, E. J.; Vlček, A., Jr. *Inorg. Chem.* **1996**, *35*, 5468.
(6) Aarnts, M. P.; Stufkens, D. J.; Vlček, A., Jr. *Inorg. Chim. Acta* **1997**, *266*, 37.
(7) Aarnts, M. P.; Stufkens, D. J.; Oskam, A.; Fraanje, J.; Goubitz, K. *Inorg. Chim. Acta* **1997**, *256*, 93.
(8) Aarnts, M. P.; Hartl, F.; Peelen, K.; Stufkens, D. J.; Amatore, C.; Verpeaux, J.-N. *Organometallics* **1997**, *16*, 4686.
(9) Aarnts, M. P.; Wilms, M. P.; Stufkens, D. J.; Baerends, E. J.; Vlček, A., Jr. *Organometallics* **1997**, *16*, 2055.
(10) Aarnts, M. P.; Oskam, A.; Stufkens, D. J.; Fraanje, J.; Goubitz, K.; Veldman, N.; Spek, A. L. *J. Organomet. Chem.* **1997**, *531*, 191.
(11) Stufkens, D. J.; Aarnts, M. P.; Nijhoff, J.; Rossenaar, B. D.; Vlček, A., Jr. *Coord. Chem. Rev.* **1998**, *171*, 93.
(12) Stufkens, D. J.; Vlček, A., Jr. *Coord. Chem. Rev.* **1998**, *177*, 127.
(13) Aarnts, M. P.; Stufkens, D. J.; Wilms, M. P.; Baerends, E. J.; Vlček, A., Jr.; Clark, I. P.; George, M. W.; Turner, J. J. *Chem.—Eur. J.* **1996**, *2*, 1556.
(14) van Slageren, J.; Stufkens, D. J. *Inorg. Chem.* **2001**, *40*, 277.
(15) van Slageren, J.; Martino, D. M.; Kleverlaan, C. J.; Bussandri, A. P.; van Willigen, H.; Stufkens, D. J. *J. Phys. Chem. A* **2000**, *104*, 5969.
(16) van Slageren, J.; Hartl, F.; Stufkens, D. J.; Martino, D. M.; van Willigen, H. *Coord. Chem. Rev.* **2000**, *208*, 309.
(17) Kleverlaan, C. J.; Stufkens, D. J. *J. Photochem. Photobiol. A* **1998**, *116*, 109.
(18) Turki, M.; Daniel, C. *Coord. Chem. Rev.* **2001**, *216−217*, 31.
(19) Weinstein, J. A.; van Slageren, J.; Stufkens, D. J.; Záliš, S.; George, M. W. *J. Chem. Soc., Dalton Trans.* **2001**, 2587.
(20) de Klerk-Engels, B.; Frühauf, H.-W.; Vrieze, K.; Kooijman, H.; Spek, A. L. *Inorg. Chem.* **1993**, *32*, 5528.

Table 1. Electronic Ground State Configurations[a] of the Investigated Complexes as Calculated by CASSCF/CASPT2 and TD-DFT

complex	GS	CASSCF/CASPT2	DFT
$[Ru(SnH_3)_2(CO)_2(Me\text{-}DAB)]$	a^1A_1	$(16a_1)(5a_2)\ (17a_1)(7b_1)(8b_1)$ $(\sigma_1)^{1.94}(d_{xy})^{1.95}(d_{y^2-z^2})^{1.95}(d_{xz})^{1.94}(\sigma_2)^{1.96}$	$(21a_1)(5a_2)\ (22a_1)(7b_1)(8b_1)$ $(\sigma_1)^2(d_{xy})^2(d_{y^2-z^2})^2(d_{xz})^2(\sigma_2)^2$
$[Ru(Me)(SnH_3)(CO)_2(Me\text{-}DAB)]$	a^1A'	$(22a')(17a'')(23a')(24a')(25a')$ $(\sigma_1)^{1.93}(d_{xy})^{1.96}(d_{y^2-z^2})^{1.95}(d_{xz})^{1.95}(\sigma_2)^{1.96}$	$(28a')(29a')(30a')(22a'')(31a')$ $(\sigma_1)^2(d_{y^2-z^2})^2(d_{xz})^2(d_{xy})^2(\sigma_2)^2$
$[Ru(Me)(Cl)(CO)_2(Me\text{-}DAB)]$	a^1A'	$(22a')\ (17a'')(23a')(24a')(25a')$ $(3p_{Cl})^2(d_{xy})^{1.96}(d_{y^2-z^2})^{1.95}(d_{xz})^{1.96}(\sigma_{MeRu})^{1.93}$	$(33a')(22a'')(34a')(35a')(23a'')$ $(d_{xz}/p_{Cl})^2(d_{xy}/p_{Cl})^2(\sigma_{MeRuCl})^2(p_{Cl}/d_{xz})^2(p_{Cl}/d_{xy})^2$ [b]
$[Ru(Cl)_2(CO)_2(Me\text{-}DAB)]$	a^1A_1	$(16a_1)(5a_2)(17a_1)(8b_1)$ $(\sigma_{ClRuCl})^{1.97}(d_{xy})^{1.97}(d_{y^2-z^2})^{1.96}(d_{xz})^{1.96}$	$(26a_1)(11b_1)(12b_1)(6a_2)$ $(d_{y^2-z^2}/p_{Cl})^2(\sigma_{ClRuCl})^2(p_{Cl}/d_{xz})^2(p_{Cl}/d_{xy})^2$ [b]

[a] Symmetry labels of the molecular orbitals are given in parentheses above the description of the corresponding electronic configurations; d_{xy}, $d_{y^2-z^2}$, and d_{xy} labels indicate molecular orbitals with more than 55% of Ru 4d contribution in the case of DFT (π^*_{DAB} and π^*_{CO} orbitals contribute the rest) and >80% of Ru 4d contribution in the case of CASSCF (π^*_{CO} orbitals contribute the rest). [b] The DFT calculated p_{Cl}/d_{xz} and p_{Cl}/d_{xy} MOs are composed approximately of 60% Cl 3p and 30% Ru 4d orbitals, while d_{xz}/p_{Cl} and d_{xy}/p_{Cl} have approximately 40% Ru 4d and 40% Cl 3p contribution. π^*_{DAB} and π^*_{CO} orbitals contribute the rest.

hexane were recorded on a Varian Cary 4E spectrophotometer. Molar absorptivities were, however, obtained in THF because of the rather low solubility of the complexes in cyclohexane. They were determined by a least-squares fitting of the absorptions measured at least at three different concentrations.

Computational Methodology

The ab initio calculations were performed on the DFT (B3LYP) optimized structures of the electronic ground states either in the C_{2v} symmetry for $[Ru(SnH_3)_2(CO)_2(Me\text{-}DAB)]$ and $[Ru(Cl)_2(CO)_2(Me\text{-}DAB)]$ or in the C_s symmetry for $[Ru(SnH_3)(Me)(CO)_2(Me\text{-}DAB)]$ and $[Ru(Cl)(Me)(CO)_2(Me\text{-}DAB)]$, see Figure 1.

The ground-state electron configurations are shown in Table 1, while the orbital characters are discussed in detail in the next section. For $[Ru(SnH_3)_2(CO)_2(Me\text{-}DAB]$, $[Ru(SnH_3)(Me)(CO)_2(Me\text{-}DAB)]$, and $[Ru(Cl)(Me)(CO)_2(Me\text{-}DAB)]$, 10 electrons were correlated in 12 active orbitals in the CASSCF calculations. These active orbitals correspond to the three 4d occupied orbitals of the Ru center, the axial σ bonding orbitals σ_1 and σ_2 and their antibonding counterparts $\sigma_{1,2}$*, the low-lying π^*_{DAB}, and the four low-lying π^*_{CO} orbitals. The CASSCF active space was restricted to 10 orbitals for $[Ru(Cl)_2(CO)_2(Me\text{-}DAB)]$: the occupied $4d_{Ru}$ orbitals, the low-lying π^*_{DAB} and four π^*_{CO} orbitals, and the σ_{ClRuCl} bonding orbital and its antibonding counterpart σ^*_{ClRuCl}. The σ bonding orbital between the Cl atoms and the $5p_x$ of the ruthenium center is too low in energy to be included in the active space and keeps the occupation number of 1.98 at the CASPT2 level. Averaged CASSCF calculations (over five roots in C_{2v} and eight roots in C_s) were performed for a given spin and symmetry in order to treat in a balanced way the various electronic states characterizing the molecules. To verify that the nearly pure $4d_{Ru}$ character of the high-lying CASSCF/CASPT2 orbitals, which differs significantly from the mixed $3p_{Cl}/4d_{Ru}$ nature of the Kohn−Sham orbitals, is not an artifact due to the size of the CASSCF active space, two extra calculations were performed for $[Ru(Cl)(Me)(CO)_2(Me\text{-}DAB)]$: (i) with 14 electrons correlated into 14 active orbitals averaged over 12 roots, and (ii) with 16 electrons correlated into 15 orbitals and averaged over 6 roots.

The CASSCF wave functions were used as references in subsequent CASPT2 calculations using the *level shift* corrected perturbation method[21] with a value of 0.2−0.3. The stability of the perturbational treatment was evaluated by performing several calculations varying the level shift values. Relativistic effective core potentials were used with the following associated valence basis sets: for the Ru atom ($Z = 16.0$), a (8s,7p,6d) set contracted to [6s,5p,3d];[22] for the Sn atoms ($Z = 4.0$), a (4s,4p) set contracted to [2s,2p];[23] for the second row atoms C ($Z = 4.0$), a (4s,4p) set contracted to [2s,2p], and O ($Z = 6.0$), a (4s,5p) set contracted to [2s,3p];[23] for the chlorine atom ($Z = 7.0$), a (4s,5p) set contracted to [2s,3p];[23] and for the H atoms, a (7s) contracted to [2s].[24] Spin−orbit coupling effects which should be very important in this molecule are not included in the present work and will be the subject of a further study. The ab initio calculations were carried out with the Molcas 4.1 and 5 systems of programs.[25] The results are analyzed in terms of CASPT2 natural orbitals.

Vertical excitation energies and transition dipole moments have also been studied using the TD-DFT method with the same basis sets on the Ru and Sn atoms in the approximation of the effective core potentials, as described above. The other atoms were described in the all-electrons scheme using the cc-pVDZ (Dunning's polarized valence double-ζ) basis set with the following contraction: [4s,3p,1d] on the Cl atom, [3s,2p,1d] on the C, O, and N atoms, and [2s,1p] on the H atom. To analyze the basis set effects on TD-DFT results for the chloride substituted complex, $[Ru(Cl)(Me)(CO)_2(Me\text{-}DAB)]$, a few calculations were performed with the basis sets described above and also with those used in the CASSCF/CASPT2 calculations or with the augmented Dunning's polarized valence double-ζ basis. The B3LYP functional was used, the exchange functional B3 being the hybrid method proposed by Becke[26] that includes a mixture of Slater exchange,[27] Becke's 1988 gradient correction,[28] and Hartree−Fock exchange. Its correlation part, LYP, is the gradient-corrected functional of Lee, Yang, and Parr.[29] The TD-DFT calculations have been performed with the GAUSSIAN98 system of programs.[30] The results for $[Ru(Cl)(Me)(CO)_2(Me\text{-}DAB)]$ were compared with those obtained using BP, B1LYP, and BLYP functionals.

Results and Discussion

Ground-State Electron Configurations. Before describing the electron configuration of the title complexes, it is important to point out that the CASSCF/CASPT2 molecular orbitals may differ significantly from the Kohn−Sham orbitals. Indeed, the DFT approach is essentially monodeterminantal, and the TD-DFT method (a linear response theory based on the ground-

(21) Roos, B. O.; Andersson, K.; Fülscher, M. P.; Serrano-Andrés, L.; Pierloot, K.; Merchán, M.; Molina, V. *THEOCHEM* **1996**, *388*, 257.

(22) Andrae, D.; Häussermann, U.; Dolg, M.; Stoll, H.; Preuss, H. *Theor. Chim. Acta* **1990**, *77*, 123.

(23) Bergner, A.; Dolg, M.; Küchle, W.; Stoll, H.; Preuss, H. *Mol. Phys.* **1993**, *80*, 1431.

(24) Pierloot, K.; Dumez, B.; Widmark, P.-O.; Roos, B. O. *Theor. Chim. Acta* **1995**, *90*, 87.

(25) Andersson, K.; Blomberg, M. R. A.; Fülscher, M. P.; Karlström, G.; Lindh, R.; Malmqvist, P.-Å.; Neogrady, P.; Olsen, J.; Roos, B. O.; Sadlej, A. J.; Schütz, M.; Seijo, L.; Serrano-Andrés, L.; Siegbahn, P. E. M.; Widmark, P.-O. *MOLCAS*, version 4.1; Lund University: Sweden, 1997.

(26) Becke, A. D. *J. Chem. Phys.* **1993**, *98*, 5648.

(27) Slater, J. C. *Quantum Theory of Molecules and Solids*; McGraw-Hill: New York, 1974.; Vol. 4.

(28) Becke, A. D. *Phys. Rev. A* **1988**, *38*, 3098.

(29) Lee, C.; Yang, W.; Parr, R. G. *Phys. Rev. B* **1988**, *37*, 785.

(30) Frisch, M. J.; Trucks, G. W.; Schlegel, H. B.; Scuseria, G. E.; Robb, M. A.; Cheeseman, J. R.; Zakrzewski, V. G.; Montgomery, J. A., Jr.; Stratmann, R. E.; Burant, J. C.; Dapprich, S.; Millam, J. M.; Daniels, A. D.; Kudin, K. N.; Strain, M. C.; Farkas, O.; Tomasi, J.; Barone, V.; Cossi, M.; Cammi, R.; Mennucci, B.; Pomelli, C.; Adamo, C.; Clifford, S.; Ochterski, J.; Petersson, G. A.; Ayala, P. Y.; Cui, Q.; Morokuma, K.; Malick, D. K.; Rabuck, A. D.; Raghavachari, K.; Foresman, J. B.; Cioslowski, J.; Ortiz, J. V.; Stefanov, B. B.; Liu, G.; Liashenko, A.; Piskorz, P.; Komaromi, I.; Gomperts, R.; Martin, R. L.; Fox, D. J.; Keith, T.; Al-Laham, M. A.; Peng, C. Y.; Nanayakkara, A.; Gonzalez, C.; Challacombe, M.; Gill, P. M. W.; Johnson, B. G.; Chen, W.; Wong, M. W.; Andres, J. L.; Head-Gordon, M.; Replogle, E. S.; Pople, J. A. *Gaussian 98*, revision A.7; Gaussian, Inc.: Pittsburgh, PA, 1998.

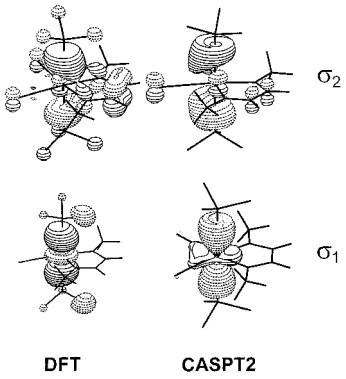

Figure 2. Comparison between Kohn−Sham (left) and CASSCF/CASPT2 (right) σ orbitals calculated for [Ru(SnH$_3$)$_2$(CO)$_2$(Me-DAB)]. (Very similar orbital shapes were obtained for [Ru(SnH$_3$)(Me)(CO)$_2$-(Me-DAB)].)

state density matrix) generates a unique set of Kohn−Sham orbitals optimized for the ground state electron density. The analysis of the transitions corresponding mainly to one-electron excitations is performed on the basis of this unique set of Kohn−Sham orbitals. In contrast, the CASSCF/CASPT2 method is multiconfigurational already at the zero order (CASSCF), and a set of natural CASPT2 orbitals optimized for each state is obtained on the basis of an average CASSCF wave function including several excited states of a given spin and symmetry. As a consequence, the Kohn−Sham orbitals will generally be more delocalized over the metal center and the ligands to compensate for the monodeterminantal picture, and the transitions will be expanded over many states. Similarly, the absolute values of the oscillator strengths will be hardly comparable, because, in the TD-DFT approach, they are calculated on the basis of a single set of Kohn−Sham orbitals, whereas, in the CASSCF method, they are obtained on the basis of a multistate scheme. In both methods, they give only qualitative estimates of transition intensities.

The electronic ground-state configurations are listed in Table 1. It is important to notice that the relative energy order of the molecular orbitals included in the CASSCF active space has no meaning, in contrast to the relative energy order of the Kohn−Sham orbitals.[31] The shapes of the relevant orbitals are depicted in Figure 2 for [Ru(SnH$_3$)$_2$(CO)$_2$(Me-DAB)], Figure 3 for the σ orbitals of [Ru(Cl)$_2$(CO)$_2$(Me-DAB] and [Ru(Cl)-(Me)(CO)$_2$(Me-DAB], and Figure 4 for the 4d$_{Ru}$ and 3p$_{Cl}$ of [Ru(Cl)(Me)(CO)$_2$(Me-DAB]. The Kohn−Sham orbitals are shown on the left, and the CASPT2 orbitals on the right.

In the case of [Ru(SnH$_3$)$_2$(CO)$_2$(Me-DAB] and [Ru(SnH$_3$)-(Me)(CO)$_2$(Me-DAB)], σ_1 represents a bonding orbital between the symmetrical combination of the sp^3-like orbitals of the Sn or C atoms of the axial ligands with the 4d$_{x^2}$ Ru orbital. The σ_2 orbital results from the antisymmetric combination of the sp^3-like orbitals of the axial ligands SnH$_3$ and Me with the 5p$_x$ Ru orbital. As shown in Figure 2, the Kohn−Sham σ_1 and σ_2 orbitals are a little more delocalized over the SnH$_3$ groups. The delocalization of σ_2 over the Me-DAB ligand is also larger for the Kohn−Sham orbital than for the case of the CASPT2 one.

The σ orbitals of [Ru(Cl)(Me)(CO)$_2$(Me-DAB)] and [Ru(Cl)$_2$-(CO)$_2$(Me-DAB)] are depicted in Figure 3. The CASPT2 σ_{MeRu} orbital is a bonding combination of the 4d$_{x^2}$ orbital of the metal center with the sp^3-like C(Me) orbital. Surprisingly, orbitals of the Cl ligand are not involved. The CASPT2 σ_{ClRuCl} orbital of [Ru(Cl)$_2$(CO)$_2$(Me-DAB)] corresponds to a symmetric combination of the 4d$_{x^2}$ orbital of the metal center with the two axial s/p(Cl) orbitals. In contrast, the Kohn−Sham σ_{MeRuCl} orbital of [Ru(Cl)(Me)(CO)$_2$(Me-DAB)] can be viewed as a weakly Cl−Ru−Me antibonding orbital that is formed by the antisymmetric combination of the s/p(Cl) orbitals and the sp^3-like C orbital of Me with the 5p$_x$(Ru) orbital. It also includes a small 4d$_{x^2}$ contribution. The Kohn−Sham σ_{ClRuCl} orbital of [Ru(Cl)$_2$(CO)$_2$-(Me-DAB)] arises from a weakly antibonding interaction between the antisymmetric combination of the s/p(Cl) orbitals of the Cl ligands and the 5p$_x$(Ru) orbital.

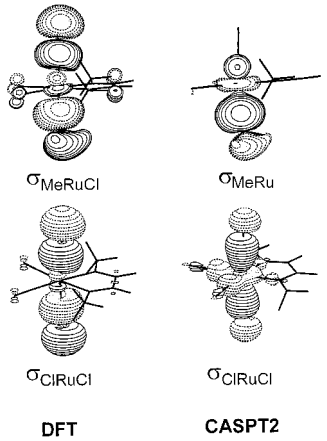

Figure 3. Comparison between Kohn−Sham (left) and CASSCF/CASPT2 (right) σ orbitals calculated for [Ru(Cl)$_2$(CO)$_2$(Me-DAB)] (bottom) and [Ru(Cl)(Me)(CO)$_2$(Me-DAB)] (top). (The Me ligand is located below the Ru(CO)$_2$(DAB) plane.)

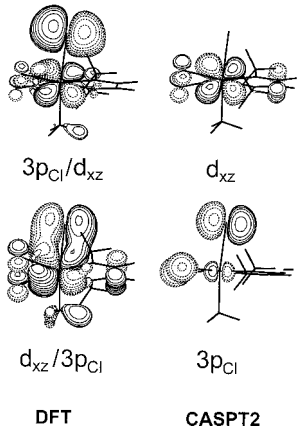

Figure 4. Comparison between Kohn−Sham (left) and CASSCF/CASPT2 (right) 4d$_{Ru}$ and 3p$_{Cl}$ orbitals calculated for [Ru(Cl)(Me)(CO)$_2$-(Me-DAB)]. (The Me ligand is located below the Ru(CO)$_2$(DAB) plane.)

In the halide complexes [Ru(Cl)(Me)(CO)$_2$(Me-DAB)] and [Ru(Cl)$_2$(CO)$_2$(Me-DAB)], the high-lying Kohn−Sham orbitals are composed of the 3p$_{Cl}$ and 4d$_{Ru}$ orbitals. The highest occupied Kohn−Sham orbitals, denoted in Table 1 as (p$_{Cl}$/d$_{xz}$) and (p$_{Cl}$/d$_{xy}$), are Ru−Cl π antibonding, as is illustrated in Figure 4 (left). Their lower-lying counterparts (d$_{xz}$/p$_{Cl}$) and (d$_{xy}$/p$_{Cl}$) are Ru−Cl π bonding. The corresponding CASPT2 orbitals (Figure 4, right) are nearly pure 4d$_{Ru}$ orbitals and do not show any significant 3p$_{Cl}$ contribution. They still exhibit the normal 4d$_{Ru}$/π^*_{CO} bonding interaction that describes the back-donation in transition metal carbonyls. These different pictures may arise from the presence of important electron correlation effects in the halide complexes. The ab initio calculations include the nondynamical part of these effects (near-degeneracy in the d-shell manifold) at the CASSCF level, whereas dynamical correlation effects originate in multiple excitations of all the

(31) Stowasser, R.; Hoffmann, R. *J. Am. Chem. Soc.* **1999**, *121*, 3414.

electrons outside the active space into the whole virtual space.[32] This is taken into account by the perturbation (CASPT2). As a consequence, the occupation numbers of the molecular orbitals involved in the electronic transitions may vary between 0 and 2. It is important to notice that $3p_{Cl}$ orbitals keep an occupation number very close to 2, in contrast to the 4d occupied orbitals for which the occupation numbers are lower, varying between 1.9 and 2.0 in the ground state. In the DFT method, these correlation effects are hardly separated and are included as a whole at the level of the correlation part of the functional. Moreover, some cancellation effects may occur.[33−35] In the case of important electronic relaxation, this essentially monodeterminantal method may have some difficulties in describing the correlation effects because of a lack of flexibility. In such situation, the Kohn−Sham orbitals will aim at compensating this drawback. These differences in the description of the high-lying occupied orbitals by the two computational strategies affect the interpretation of electronic transitions of the halide complexes, as will be discussed later in this work.

It should be noted at this point that details of the orbital picture may vary depending on the CASSCF active space (see the Computational Methodology section), on the quality of the basis set, and on the DFT functional, as will be discussed elsewhere.[36] For instance, the $3p_{Cl}$ orbitals remain predominantly pure (64% as compared to 70% in the standard calculation) with a very small contribution of the $4d_{Ru}$ orbitals (less than 5%) even if they are included in the CASSCF active space (CASSCF 14e14a or 16e15a). The values of the occupation numbers of the electronic ground-state CASPT2 natural orbitals (1.9445 for the $4d_{Ru}$ orbital and 1.994 for the $3p_{Cl}$ orbital) illustrate the weak correlation of the $3p_{Cl}$ electrons as compared with the $4d_{Ru}$ electrons. Similarly, in DFT, the $3p_{Cl}$ contribution to the high-lying $3p_{Cl}/4d_{Ru}$ orbital may vary between 60% (with the B3LYP functional) and 80% (with a BP functional).

The low-lying vacant orbitals of all four complexes are of a π^*_{DAB} and π^*_{CO} character, localized predominantly on the DAB and CO acceptor ligands, respectively. They are followed in energy by the antibonding counterparts of the σ bonding orbitals defined previously.

Experimental Absorption Spectra. The UV−visible absorption spectra of the complexes $[Ru(SnPh_3)_2(CO)_2(iPr\text{-}DAB)]$, $[Ru(SnPh_3)(Me)(CO)_2(iPr\text{-}DAB)]$, $[Ru(Cl)(Me)(CO)_2(iPr\text{-}DAB)]$, and $[Ru(Cl)_2(CO)_2(iPr\text{-}DAB)]$ obtained from cyclohexane solutions are reported in Figures 5−8. It is assumed that the transition energies measured in the nonpolar cyclohexane solvent will approach those expected in the vacuum. Molar absorptivities were determined in THF for solubility reasons. The corresponding values are listed in Tables 2−5, together with the computational results.

The complexes $[Ru(SnPh_3)_2(CO)_2(iPr\text{-}DAB)]$ and $[Ru(SnPh_3)(Me)(CO)_2(iPr\text{-}DAB)]$ have rather similar absorption spectra. They show a strong absorption band at 529 and 539 nm (i.e., 18 900 and 18 550 cm^{-1}), respectively. Absorption is very weak between ∼460 and 340 nm. Herein, a weak, broad band at ∼400 nm (25 000 cm^{-1}) was found for $[Ru(SnPh_3)_2(CO)_2(iPr\text{-}DAB)]$ while $[Ru(SnPh_3)(Me)(CO)_2(iPr\text{-}DAB)]$ displays a weak shoulder at 450 nm (22 220 cm^{-1}) and a weak, but distinct, band at 394 nm (25 380 cm^{-1}). In the far-UV region, $[Ru(SnPh_3)_2(CO)_2(iPr\text{-}DAB)]$ shows a strong, sharp band at 310 nm (32 260 cm^{-1}), which is absent in the spectrum of $[Ru(SnPh_3)(Me)$-

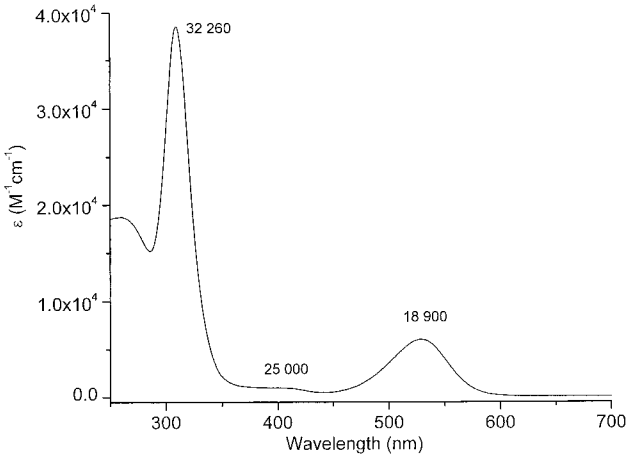

Figure 5. UV-visible absorption spectra of $[Ru(SnPh_3)_2(CO)_2(iPr\text{-}DAB)]$ in a cyclohexane solution. The abscissa shows the molar absorptivity measured in THF. Inset numbers specify wavenumbers of the absorption maxima in reciprocal centimeters.

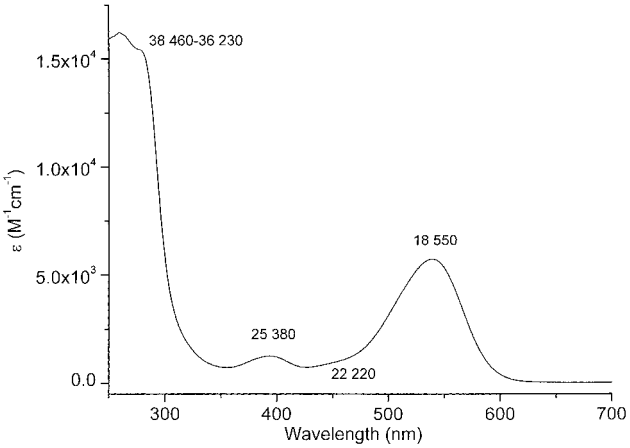

Figure 6. UV−visible absorption spectra $[Ru(SnPh_3)(Me)(CO)_2(iPr\text{-}DAB)]$ in a cyclohexane solution. The abscissa shows the molar absorptivity measured in THF. Inset numbers specify wavenumbers of the absorption maxima in reciprocal centimeters.

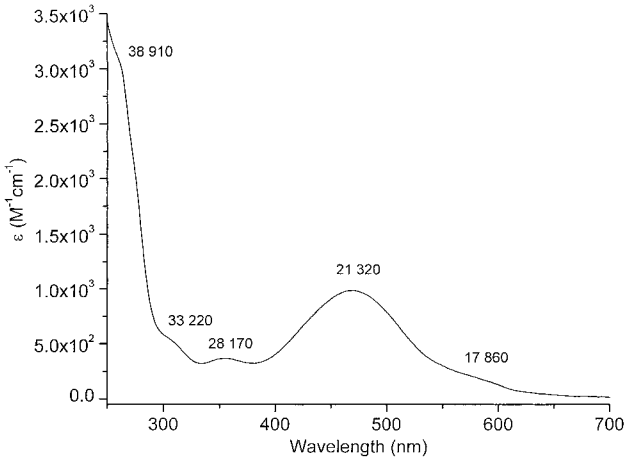

Figure 7. UV−visible absorption spectra in cyclohexane of $[Ru(Cl)_2(CO)_2(iPr\text{-}DAB)]$. The abscissa shows the molar absorptivity measured in THF. Inset numbers specify wavenumbers of the absorption maxima in reciprocal centimeters.

(32) Martin, C. H.; Zerner, M. C. In *Inorganic Electronic Structure and Spectroscopy, Volume I: Methodology*; Solomon, E. I., Lever, A. B. P., Eds.; John Wiley & Sons: New York, 1999; p 555.

(33) Li, J.; Noodleman, L.; Case, D. A. In *Inorganic Electronic Structure and Spectroscopy, Volume I: Methodology*; Solomon, E. I., Lever, A. B. P., Eds.; J. Wiley & Sons: New York, 1999; p 661.

(34) Baerends, E. J.; Gritsenko, O. V. *J. Phys. Chem. A* **1997**, *101*, 5383.

(35) Chermette, H. *Coord. Chem. Rev.* **1998**, *178−180*, 699.

(36) Záliš, S.; Benamor, N.; Bossert, J.; Daniel, C. *Chem. Phys. Lett.*, in preparation.

Table 2. Experimental Absorption Maxima of $[Ru(SnPh_3)_2(CO)_2(iPr\text{-}DAB)]$ and CASSCF/CASPT2 and TD-DFT Calculated Excitation Energies and Assignments of Low-Lying Electronic Transitions of $[Ru(SnH_3)_2(CO)_2(Me\text{-}DAB)]$[a]

experiment	CASSCF/CASPT2	TD-DFT
	visible	
18 900 (6050)	21 260 (0.17) b^1A_1: 70% $\sigma_2 \rightarrow \pi^*_{DAB}$	22 020 (0.063) b^1A_1: 75% $\sigma_2 \rightarrow \pi^*_{DAB}$
	near UV	
25 000 (960)	24 630 (0.005) a^1B_2: 77% $d_{xy} \rightarrow \pi^*_{DAB}$	24 680 (0.006) a^1B_2: 92% $d_{xy} \rightarrow \pi^*_{DAB}$
	UV	
32 260 (38 500)	29 220 (0.13) c^1A_1: 70% $d_{xz} \rightarrow \pi^*_{DAB}$	29 760 (0.042) c^1A_1: 87% $d_{xz} \rightarrow \pi^*_{DAB}$
	32 940 (0.003) a^1B_1: 72% $d_{y^2-z^2} \rightarrow \pi^*_{DAB}$	30 410 (0.01) a^1B_1: 98% $d_{y^2-z^2} \rightarrow \pi^*_{DAB}$
	33 930 (0.018) b^1B_1: 68% $\sigma_1 \rightarrow \pi^*_{DAB}$	32 182 (0.002) b^1B_1: 77% $\sigma_1 \rightarrow \pi^*_{DAB}$
		18% $\sigma_2 \rightarrow \pi^*_{CO}$
	far UV	
~38 460 (18 700)	37 330 (0.005) c^1B_1: 66% $d_{xy} \rightarrow \pi^*_{CO}$	36 540 (0.098) c^1B_1: 76% $\sigma_2 \rightarrow \pi^*_{CO}$
	38 360 (0.13) d^1B_1: 52% $\sigma_2 \rightarrow \pi^*_{CO}$	37 590 (0.045) d^1B_1: 72% $d_{xy} \rightarrow \pi^*_{CO}$
	39 640 (0.003) b^1B_2: 50% $\sigma_2 \rightarrow \pi^*_{CO}$	16% $\sigma_2 \rightarrow \pi^*_{CO}$
	21% $\sigma_1 \rightarrow \pi^*_{CO}$	38 630 (0.132) e^1B_1: 54% $\sigma_2 \rightarrow \pi^*_{CO}$
		10% $d_{xy} \rightarrow \pi^*_{CO}$
		39 760 (0.004) b^1B_2: 50% $\sigma_2 \rightarrow \pi^*_{CO}$

[a] Energies in cm^{-1}. Experimental molar absorptivities ($M^{-1}cm^{-1}$) and calculated oscillator strengths are given in parentheses. Electronic transitions from the a^1A_1 ground state to specified excited states are described by principal contributing orbital excitations, greater than 10%.

Table 3. Experimental Absorption Maxima of $[Ru(SnPh_3)(Me)(CO)_2(iPr\text{-}DAB)]$ and CASSCF/CASPT2 and TD-DFT Calculated Excitation Energies and Assignments of Low-Lying Electronic Transitions of $[Ru(SnH_3)(Me)(CO)_2(Me\text{-}DAB)]$[a]

experiment	CASSCF/CASPT2	TD-DFT
	visible	
18 550 (5710)	20 400 (0.11), b^1A': 61% $\sigma_2 \rightarrow \pi^*_{DAB}$	21 530 (0.06), b^1A': 70% $\sigma_2 \rightarrow \pi^*_{DAB}$
		10% $d_{xz} \rightarrow \pi^*_{DAB}$
22 220 (930)	20 750 (0.004), a^1A'': 76% $d_{xy} \rightarrow \pi^*_{DAB}$	21 700 (0.002), a^1A'': 94% $d_{xy} \rightarrow \pi^*_{DAB}$
	near UV	
25 380 (1250)	25 690 (0.22), c^1A': 67% $d_{xz} \rightarrow \pi^*_{DAB}$	27 340 (0.067), c^1A': 81% $d_{xz} \rightarrow \pi^*_{DAB}$
	UV	
no absorption	31 260 (0.000), d^1A': 80% $d_{y^2-z^2} \rightarrow \pi^*_{DAB}$	28 960 (0.001), d^1A': 98% $d_{y^2-z^2} \rightarrow \pi^*_{DAB}$
	far UV	
36 230−39 500	35 260 (0.000), b^1A'': 53% $\sigma_2 \rightarrow \pi^*_{CO}$	33 230 (0.000), b^1A'': 96% $\sigma_2 \rightarrow \pi^*_{CO}$
(15 440−16 220)	35 880 (0.03), e^1A': 61% $\sigma_1 \rightarrow \pi^*_{DAB}$	35 400 (0.000), e^1A': 58% $\sigma_1 \rightarrow \pi^*_{DAB}$
		17% $\sigma_2 \rightarrow \pi^*_{CO}$
	36 820 (0.003), f^1A': 66% $d_{xy} \rightarrow \pi^*_{CO}$	36 620 (0.002), f^1A': 74% $d_{xy} \rightarrow \pi^*_{CO}$
	38 710 (0.000), c^1A'': 51% $d_{xz} \rightarrow \pi^*_{DAB}$	37 180 (0.047), g^1A': 63% $\sigma_2 \rightarrow \pi^*_{CO}$
	17% $\sigma_2 \rightarrow \pi^*_{CO}$	10% $\sigma_1 \rightarrow \pi^*_{DAB}$
	39 200 (0.05), g^1A': 53% $\sigma_2 \rightarrow \pi^*_{CO}$	

[a] Energies in cm^{-1}. Experimental molar absorptivities ($M^{-1}cm^{-1}$) and calculated oscillator strengths are given in parentheses. Electronic transitions from the a^1A' ground state to specified excited states are described by principal contributing orbital excitations, greater than 10%.

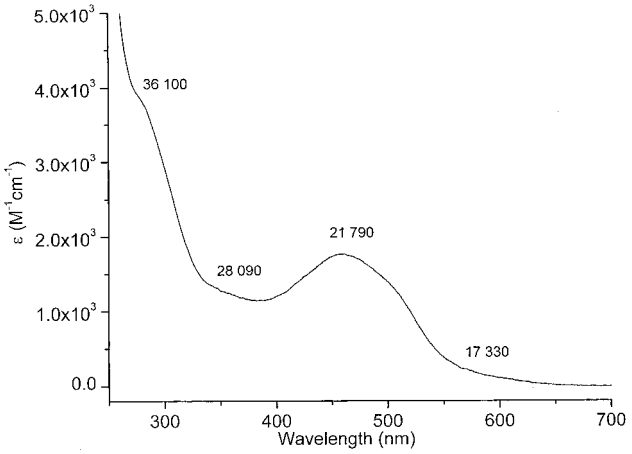

Figure 8. UV−visible absorption spectra of $[Ru(Cl)(Me)(CO)_2(iPr\text{-}DAB)]$ in a cyclohexane solution. The abscissa shows the molar absorptivity measured in THF. Inset numbers specify wavenumbers of the absorption maxima in reciprocal centimeters.

$(CO)_2(iPr\text{-}DAB)]$. Both complexes display a broad, intense absorption in the region 300−250 nm (33 330−40 000 cm^{-1}), which is composed of several overlapping bands.

The lowest-energy visible absorption band of the halide complexes $[Ru(Cl)(Me)(CO)_2(iPr\text{-}DAB)]$ and $[Ru(Cl)_2(CO)_2(iPr\text{-}DAB)]$ occurs at higher energies, 459 and 469 nm (21 790 and 21 320 cm^{-1}), respectively. It is ~3 and 6 times weaker than the visible band observed for $[Ru(SnPh_3)(Me)(CO)_2(iPr\text{-}DAB)]$ and $[Ru(SnPh_3)_2(CO)_2(iPr\text{-}DAB)]$. An absorption "tail" is seen on the red side of the main visible band of both species. $[Ru(Cl)(Me)(CO)_2(iPr\text{-}DAB)]$ shows a broad absorption between 400 and 300 nm with an unresolved shoulder at ~356 nm (28 090 cm^{-1}), while a weak band at 355 nm (28 170) and a distinct shoulder at 301 nm (33 220 cm^{-1}) occur in the spectrum of $[Ru(Cl)_2(CO)_2(iPr\text{-}DAB)]$. For both complexes, strong absorption follows in the region 280−250 nm (35 710−40 000 cm^{-1}), extending further into the UV region.

Assignment of Absorption Bands. The energies of the transitions to singlet excited states of $[Ru(E)(E')(CO)_2(Me\text{-}DAB)]$ (E = E′ = SnH_3 or Cl; E = SnH_3 or Cl, E′ = Me) calculated at the CASSCF/CASPT2 and TD-DFT levels are reported in Tables 2−5, together with the oscillator strengths and the percentages of principal contributing one-electron excitations. Electronic spectra will be discussed in terms of four energy domains for which experimental data are available: (i) the visible region below 25 000 cm^{-1}; (ii) the near-UV energy

Table 4. Experimental Absorption Maxima of $[Ru(Cl)_2(CO)_2(iPr\text{-}DAB)]$ and CASSCF/CASPT2 and TD-DFT Calculated Excitation Energies and Assignments of Low-Lying Electronic Transitions of $[Ru(Cl)_2(CO)_2(Me\text{-}DAB)]$[a]

experiment	CASSCF/CASPT2	TD-DFT
	visible	
17 860 (w, sh)	19 630 (0.007), a^1B_2: 91% $d_{xy} \rightarrow \pi^*_{DAB}$	14 840 (0.000), a^1B_2: 98% $p_{Cl}/d_{xy} \rightarrow \pi^*_{DAB}$
21 320 (990)	22 730 (0.12), b^1A_1: 90% $d_{xz} \rightarrow \pi^*_{DAB}$	16 540 (0.013), b^1A_1: 94% $p_{Cl}/d_{xz} \rightarrow \pi^*_{DAB}$
	near UV	
28 170 (370)	29 070 (0.009), a^1B_1: 81% $d_{xz} \rightarrow \sigma^*_{ClRuCl}$ 14% $d_{xy} \rightarrow d_{yz}$	26 540 (0.001), a^1B_1: 89% $p_{Cl}/d_{xz} \rightarrow \sigma^*_{ClRuCl}$
	31 850 (0.000), b^1B_1: 87% $d_{y^2-z^2} \rightarrow \pi^*_{DAB}$	28 960 (0.000), b^1B_1: 97% $d_{y^2-z^2} \rightarrow \pi^*_{DAB}$
	UV	
33 220 (580)	36 130 (0.003), c^1B_1: 77% $d_{xy} \rightarrow d_{yz}$	31 200 (0.000), b^1B_2: 89% $d_{xy}/p_{Cl} \rightarrow \pi^*_{DAB}$ 13% $d_{xz} \rightarrow \sigma^*_{ClRuCl}$
	far UV	
>38 910 (>3270)	39 840 (0.27), c^1B_2: 91% $d_{xy} \rightarrow \pi^*_{CO}$	31 400 (0.002), d^1B_1: 87% $p_{Cl}/d_{xy} \rightarrow \pi^*_{CO}$

[a] Energies in cm^{-1}. Experimental molar absorptivities ($M^{-1}cm^{-1}$) and calculated oscillator strengths are given in parentheses. Electronic transitions from the a^1A_1 ground state to specified excited states are described by principal contributing orbital excitations, greater than 10%.

Table 5. Experimental Absorption Maxima of $[Ru(Cl)(Me)(CO)_2(iPr\text{-}DAB)]$ and CASSCF/CASPT2 and TD-DFT Calculated Excitation Energies and Assignments of Low-Lying Electronic Transitions of $[Ru(Cl)(Me)(CO)_2(Me\text{-}DAB)]$[a]

experiment	CASSCF/CASPT2	TD-DFT
	visible	
17 330 (sh, w)	17 890 (0.005), a^1A'': 80% $d_{xy} \rightarrow \pi^*_{DAB}$	14 440 (0.000), a^1A'': 96% $p_{Cl}/d_{xy} \rightarrow \pi^*_{DAB}$
21 790 (1760)	22 630 (0.23), b^1A': 65% $d_{xz} \rightarrow \pi^*_{DAB}$ 19% $\sigma_{MeRu} \rightarrow \pi^*_{DAB}$	16 210 (0.011), b^1A': 91% $p_{Cl}/d_{xz} \rightarrow \pi^*_{DAB}$
	near UV	
28 090 (1240)	26 830 (0.038), c^1A': 62% $\sigma_{MeRu} \rightarrow \pi^*_{DAB}$ 16% $d_{xz} \rightarrow \pi^*_{DAB}$	23 310 (0.015), c^1A': 87% $\sigma_{MeRuCl} \rightarrow \pi^*_{DAB}$
		24 720 (0.000), b^1A'': 96% $d_{xy}/p_{Cl} \rightarrow \pi^*_{DAB}$
	UV	
no absorption	30 520 (0.002), d^1A': 87% $d_{y^2-z^2} \rightarrow \pi^*_{DAB}$	27 100 (0.000), d^1A': 98% $d_{y^2-z^2} \rightarrow \pi^*_{DAB}$
	far UV	
>36 100 (>3870)	35 400 (0.001), e^1A': 77% $d_{xy} \rightarrow \pi^*_{CO}$	27 500 (0.060), e^1A': 88% $d_{xz}/p_{Cl} \rightarrow \pi^*_{DAB}$
	35 530 (0.008), c^1A'': 61% $d_{xy} \rightarrow \pi^*_{CO}$	32 600 (0.002), f^1A': 87% $p_{Cl}/d_{xy} \rightarrow \pi^*_{CO}$
	36 130 (0.000), b^1A'': 66% $d_{y^2-z^2} \rightarrow \pi^*_{CO}$ 16% $d_{xy} \rightarrow \pi^*_{CO}$	33 800 (0.000), c^1A'': 52% $p_{Cl}/d_{xz} \rightarrow \pi^*_{CO}$ 37% $p_{Cl}/d_{xy} \rightarrow \pi^*_{CO}$

[a] Energies in cm^{-1}. Experimental molar absorptivities ($M^{-1}cm^{-1}$) and calculated oscillator strengths are given in parentheses. Electronic transitions from the a^1A' ground state to specified excited states are described by principal contributing orbital excitations, greater than 10%.

Table 6. Changes in Mulliken Populations upon the First Allowed Electronic Transitions of the Model Complexes $[Ru(E)(E')(CO)_2(Me\text{-}DAB)]$ Calculated by CASPT2 and TD-DFT

complex	state	method	Ru	E	E′	$(CO)_2$	Me-DAB
E = SnH_3 E′ = SnH_3	b^1A_1	CASPT2	−0.161	0.039	0.039	−0.016	0.099
		TD DFT	−0.061	−0.140	−0.140	−0.092	0.433
E = SnH_3 E′ = Me	b^1A'	CASPT2	−0.187	0.058	0.008	−0.027	0.148
		TD DFT	−0.083	−0.195	−0.138	−0.095	0.511
E = Me E′ = Cl	b^1A'	CASPT2	−0.212	−0.076	−0.073	−0.162	0.523
		TD DFT	−0.163	−0.005	−0.612	−0.006	0.786
E = Cl E′ = Cl	b^1A_1	CASPT2	−0.225	−0.140	−0.140	−0.150	0.655
		TD DFT	−0.236	−0.298	−0.298	0.004	0.828

domain between 25 000 and 30 000 cm^{-1}; (iii) the UV region between 30 000 and 35 000 cm^{-1}; and (iv) the far-UV spectrum domain between 35 000 and 40 000 cm^{-1}. Higher-lying transitions are not discussed herein. The spectral assignment is based on a comparison of experimental band maxima with calculated energies of transitions with significant oscillator strengths. However, oscillator strengths should be used rather qualitatively, to distinguish allowed transitions from forbidden, very weak transitions to other excited states that also occur in the relevant energy regions. In general, the electronic transitions are analyzed in terms of contributing orbital excitations. Moreover, the lowest allowed electronic transitions are described by accompanying changes in Mulliken populations, which are summarized in Table 6.

$[Ru(SnH_3)_2(CO)_2(Me\text{-}DAB)]$ and $[Ru(SnH_3)(Me)(CO)_2(Me\text{-}DAB)]$. The agreement between CASSCF/CASPT2 and TD-DFT results obtained for these two model complexes is very good, see Tables 2 and 3. The calculated values correspond well to the experimental spectra (Figures 5 and 6) of the two nonhalide complexes investigated.

The lowest-energy part of the absorption spectra of both complexes originates in an electronic transition that corresponds to excitation from the axial E−Ru−SnH_3 (E = SnH_3 or Me) σ_2 orbital into the low-lying π^*_{DAB} orbital localized predominantly on Me-DAB (SBLCT transition). The first intense band observed at 18 900 cm^{-1} and 18 550 cm^{-1} for $[Ru(SnPh_3)_2(CO)_2(iPr\text{-}DAB)]$ and $[Ru(SnPh_3)(Me)(CO)_2(iPr\text{-}DAB)]$, respectively, can thus be assigned to SBLCT transitions to the

respective b^1A_1 and b^1A' SBLCT states. These transitions were calculated by CASSCF/CASPT2 for the corresponding model complexes $[Ru(SnH_3)_2(CO)_2(Me\text{-}DAB)]$ and $[Ru(SnH_3)(Me)(CO)_2(Me\text{-}DAB)]$ at 21 260 cm^{-1} and 20 400 cm^{-1}, with high oscillator strengths. TD-DFT confirms this assignment. The changes in Mulliken population on excitation (Table 6) further support the description of the lowest allowed electronic transitions of $[Ru(SnPh_3)_2(CO)_2(iPr\text{-}DAB)]$ and $[Ru(SnPh_3)(Me)(CO)_2(iPr\text{-}DAB)]$ as SBLCT. However, it is interesting to notice that TD-DFT predicts a much larger charge redistribution on SBLCT excitation than CASSCF/CASPT2. This is manifested by a much larger population increase on Me-DAB and decrease on the E ligands, as calculated by TD-DFT. In contrast, CASSCF/CASPT2 only predicts a large population decrease on Ru. Hence, the TD-DFT description is closer to the SBLCT one, while CASSCF/CASPT2 indicates a more delocalized type of an electronic transition, despite the fact that the CASSCF/CASPT2 molecular orbitals are more localized. This is due to configuration interaction.

The near-UV and UV regions of the spectra consist mainly of transitions to MLCT or SBLCT states. This is the case for the very weak shoulders observed at 25 000 cm^{-1} and at ~22 220 cm^{-1} for $[Ru(SnPh_3)_2(CO)_2(iPr\text{-}DAB)]$ and $[Ru(SnPh_3)(Me)(CO)_2(iPr\text{-}DAB)]$, respectively; see Figures 5 and 6. They are assigned to transitions to the a^1B_2 and a^1A'' states, respectively, which have the principal contributing excitation $4d_{xy} \rightarrow \pi^*_{DAB}$. Besides that, $[Ru(SnH_3)_2(CO)_2(Me\text{-}DAB)]$ was calculated to have a strong $a^1A_1 \rightarrow c^1A_1$ MLCT transition of a predominant $4d_{xz} \rightarrow \pi^*_{DAB}$ character at higher energies: 29 220 cm^{-1} (CASSCF/CASPT2) or 29 760 cm^{-1} (TD-DFT). This transition accounts for the sharp, intense 310 nm (32 260 cm^{-1}) band specific for $[Ru(SnPh_3)_2(CO)_2(iPr\text{-}DAB)]$. A strong MLCT transition of the same $4d_{xz} \rightarrow \pi^*_{DAB}$ character was calculated for $[Ru(SnH_3)(Me)(CO)_2(Me\text{-}DAB)]$ at 25 690 cm^{-1} (CASSCF/CASPT2) or 27 340 cm^{-1} (TD-DFT). However, this transition cannot be directly located in the experimental spectrum of $[Ru(SnPh_3)(Me)(CO)_2(iPr\text{-}DAB)]$, Figure 6. It is probably responsible for the 394 nm band (25 380 cm^{-1}). This assignment would imply, however, that the calculated oscillator strengths are much overestimated by both methods. Apart from this, the absence of any strong UV absorption of $[Ru(SnPh_3)(Me)(CO)_2(iPr\text{-}DAB)]$ up until ~38 460 cm^{-1} is confirmed by the zero oscillator strength of the transition to the d^1A' state calculated at 31 260 cm^{-1} and by the weakness of all SBLCT and MLCT transitions directed either to π^*_{CO} or π^*_{DAB} orbitals, which were calculated to occur in the 35 000−37 000 cm^{-1} range.

Above 35 000 cm^{-1}, the transitions of $[Ru(SnH_3)_2(CO)_2(Me\text{-}DAB)]$ correspond to excitations into the π^*_{CO} orbitals localized on the carbonyl ligands, either from $4d_{Ru}$ orbitals or from $\sigma_{E-Ru-E'}$ orbitals. Out of the three nearly degenerate transitions calculated in the vicinity of the experimental band in the region 38 000−40 000 cm^{-1}, only the $a^1A_1 \rightarrow d^1B_1$ SBLCT transition directed to π^*_{CO} has a large CASSCF-calculated oscillator strength (0.13). Hence, this transition is assigned as the principal contributor to the 260 nm (38 460 cm^{-1}) absorption band of $[Ru(SnPh_3)_2(CO)_2(iPr\text{-}DAB)]$. The TD-DFT method attributes this absorption band to three mixed-character SBLCT and MLCT transitions which are directed into π^*_{CO} orbitals: $a^1A \rightarrow c^1B_1$, d^1B_1, and e^1B_1.

The description of the UV absorption spectrum of $[Ru(SnH_3)(Me)(CO)_2(Me\text{-}DAB)]$ above 35 000 cm^{-1} is more problematic. However, the number and variety of transitions with low oscillator strengths calculated in this energy region reflect the trend in the experimental spectra upon substituting one $SnPh_3$ group in $[Ru(SnPh_3)_2(CO)_2(iPr\text{-}DAB)]$ for a methyl ligand, namely, the fact that a single intense band at 260 nm splits into three bands at 260, 265, and 276 nm for $[Ru(SnPh_3)(Me)(CO)_2(iPr\text{-}DAB)]$. These three bands can be assigned to transitions into the e^1A' SBLCT, f^1A' MLCT, and g^1A' SBLCT states, which were calculated by CASSCF/CASPT2 with nonzero oscillator strengths at 35 880 cm^{-1}, 36 820 cm^{-1}, and 39 200 cm^{-1}, respectively, for the model complex. In contrast, TD-DFT predicts only one strong transition to occur in this energy domain, at 37 180. It is $a^1A' \rightarrow g^1A'$, which has SBLCT character, being directed to π^*_{CO} orbitals.

In summary, both CASSCF/CASPT2 and TD-DFT calculations reproduce well the electronic absorption spectra of $[Ru(SnPh_3)_2(CO)_2(iPr\text{-}DAB)]$ and $[Ru(SnPh_3)(Me)(CO)_2(iPr\text{-}DAB)]$. Namely, very good agreement was achieved concerning the energy and character of the strong visible absorption band, because of $\sigma_2 \rightarrow \pi^*_{DAB}$ SBLCT excitation. This interpretation agrees well with the previous experimental assignment.[5,13] Both techniques only slightly overestimate the transition energy, while the small red-shift observed on going from $[Ru(SnPh_3)_2(CO)_2(iPr\text{-}DAB)]$ to $[Ru(SnPh_3)(Me)(CO)_2(iPr\text{-}DAB)]$ is well accounted for. The absence of absorption in the near UV region is also well reproduced computationally, because the MLCT transitions, which occur herein, were calculated to have rather low oscillator strengths. The only calculated strong MLCT transition has $4d_{xz} \rightarrow \pi^*_{DAB}$ excitation as its principal component. For $[Ru(SnPh_3)_2(CO)_2(iPr\text{-}DAB)]$, it is manifested by the strong band at 310 nm. Interestingly, both computational techniques have revealed a dense manifold of MLCT and SBLCT transitions which involve electron excitation from $4d_{Ru}$ orbitals or the σ_2 orbital into π^*_{CO} orbitals. These transitions occur above 35 000 cm^{-1} (285 nm) where both complexes indeed show a strong absorption.

$[Ru(Cl)(Me)(CO)_2(Me\text{-}DAB)]$ and $[Ru(Cl)_2(CO)_2(Me\text{-}DAB)]$. The CASSCF/CASPT2 and TD-DFT approaches lead to different descriptions of electronic transitions of the halide complexes $[Ru(Cl)(Me)(CO)_2(Me\text{-}DAB)]$ and $[Ru(Cl)_2(CO)_2(Me\text{-}DAB)]$. The computational results of both techniques are summarized in Tables 4 and 5.

CASSCF/CASPT2 reproduces well the observed blue-shift of the lowest allowed absorption band on going from the nonhalide to the halide complexes. The calculated transition energies are only slightly higher than the experimental absorption band maxima. The $4d_{xz} \rightarrow \pi^*_{DAB}$ MLCT excitation has been identified as the main contributor to the lowest allowed transition into the b^1A_1 or b^1A' excited states of $[Ru(Cl)_2(CO)_2(Me\text{-}DAB)]$ and $[Ru(Cl)(Me)(CO)_2(Me\text{-}DAB)]$, respectively. This transition was calculated at 22 630 cm^{-1} with an oscillator strength of 0.23 for $[Ru(Cl)(Me)(CO)_2(Me\text{-}DAB)]$ and at 22 730 cm^{-1} with an oscillator strength of 0.12 for $[Ru(Cl)_2(CO)_2(Me\text{-}DAB)]$. A very weak MLCT transition was calculated at 17 890 cm^{-1} and 19 630 cm^{-1} for $[Ru(Cl)(Me)(CO)_2(Me\text{-}DAB)]$ and $[Ru(Cl)_2(CO)_2(Me\text{-}DAB)]$, respectively. They are directed into the excited states a^1A'' and a^1B_2, respectively, and may contribute to the weak absorption tail detected at ~577 nm (17 330 cm^{-1}) and 560 nm (17 860 cm^{-1}) in the spectra of the corresponding complexes $[Ru(Cl)(Me)(CO)_2(iPr\text{-}DAB)]$ and $[Ru(Cl)_2(CO)_2(iPr\text{-}DAB)]$, see Figures 7 and 8. Analysis in terms of Mulliken population changes corroborates the CASSCF/CASPT2 description of the lowest allowed transition as predominantly MLCT. Data in Table 6 clearly demonstrate the characteristic large decrease of population at the $Ru(CO)_2$ moiety and a rise in population at the Me-DAB ligands. The population decrease at

the Cl ligand(s), albeit low, is present, especially for $[Ru(Cl)_2(CO)_2(iPr\text{-}DAB)]$.

The weak band at 28 170 cm^{-1} (355 nm) observed for $[Ru(Cl)_2(CO)_2(Me\text{-}DAB)]$ is attributed to $a^1A_1 \rightarrow a^1B_1$ MSBCT (metal-to-σ-bond charge transfer) transition with a $4d_{xz} \rightarrow \sigma^*_{ClRuCl}$ main component. The 28 090 cm^{-1} (356 nm) shoulder superimposed on the broad UV absorption of $[Ru(Cl)(Me)(CO)_2(iPr\text{-}DAB)]$ belongs to the $a^1A' \rightarrow c^1A'$ SBLCT ($\sigma_{MeRu} \rightarrow \pi^*_{DAB}$) transition. MLCT transitions into the d^1A' ($[Ru(Cl)(Me)(CO)_2(Me\text{-}DAB)]$) and b^1B_1 ($[Ru(Cl)_2(CO)_2(Me\text{-}DAB)]$) states correspond to $4d_{y^2-z^2} \rightarrow \pi^*_{DAB}$ excitation. They were calculated at 30 520 cm^{-1} and 31 850 cm^{-1}, respectively, and are probably responsible for the weak, unresolved UV absorption observed for $[Ru(Cl)(Me)(CO)_2(iPr\text{-}DAB)]$ and $[Ru(Cl)_2(CO)_2(iPr\text{-}DAB)]$. The far-UV part of the calculated absorption spectra of $[Ru(Cl)(Me)(CO)_2(Me\text{-}DAB)]$ and $[Ru(Cl)_2(CO)_2(Me\text{-}DAB)]$ consists mainly of MLCT transitions derived from excitations into low-lying π^*_{CO} orbitals. Namely, a very intense absorption at 39 840 cm^{-1} attributed to transition to the c^1B_2 state was calculated for $[Ru(Cl)_2(CO)_2(Me\text{-}DAB)]$. The first MC (metal-centered) transition calculated for $[Ru(Cl)_2(CO)_2(Me\text{-}DAB)]$ is directed to the c^1B_1 state. It occurs at 36 130 cm^{-1} with a very low oscillator strength of 0.003. The $4d_{xy} \rightarrow 4d_{yz}$ excitation contributes 77% to this MC transition, which may be responsible for the shoulder at 33 220 cm^{-1}. No analogous MC transition was calculated for $[Ru(Cl)(Me)(CO)_2(Me\text{-}DAB)]$ or observed in the spectrum of $[Ru(Cl)(Me)(CO)_2(iPr\text{-}DAB)]$.

TD-DFT systematically underestimates the transition energies of the halide complexes, although the general spectral pattern is well reproduced, see Tables 4 and 5. In contrast to the experiment, TD-DFT predicts the lowest allowed electronic transition in the halide complexes $[Ru(Cl)(Me)(CO)_2(Me\text{-}DAB)]$ and $[Ru(Cl)_2(CO)_2(Me\text{-}DAB)]$ to occur at lower energies than for the nonhalide species. On the other hand, TD-DFT reproduces well the increase of molar absorptivity of the visible absorption band on going from the halide to the nonhalide complexes.

A careful analysis of the Kohn−Sham orbitals shows that the high-lying occupied orbitals of the halide complexes have mixed $4d_{Ru}/3p_{Cl}$ character and are Ru−Cl π antibonding, vide supra. The halide contribution is rather large, ~60%. This result contrasts with the high-lying occupied orbitals calculated by CASSF/CASPT2 which are strongly Ru-localized, of a predominantly 4d character. (The orbital shapes are compared in Figure 4.) Consequently, the lowest allowed electronic transitions of the halide complexes are described by TD-DFT as originating predominantly in a $3p_{Cl}/4d_{xz} \rightarrow \pi^*_{DAB}$ excitation. Such an electronic transition can be best described as a mixed XLCT/MLCT one, (XLCT = halide-to-ligand charge transfer).[1−3,12] By contrast, CASSCF/CASPT2 views this transition as an essentially pure MLCT. Similarly, all higher-lying transitions described as MLCT by CASSCF/CASPT2 are interpreted as mixed XLCT/MLCT by TD-DFT. The assignment of the weak UV band of $[Ru(Cl)(Me)(CO)_2(iPr\text{-}DAB)]$ (28 090 cm^{-1}) to a $\sigma \rightarrow \pi^*$ transition is similar in both techniques, as is the assignment of the similar weak UV band of $[Ru(Cl)_2(CO)_2(iPr\text{-}DAB)]$ (at 28 170 cm^{-1}) to an MSBCT transition. However, TD-DFT indicates that a $p_{Cl} \rightarrow \sigma^*$ excitation also contributes to the latter transition through the p_{Cl}/d_{xz} mixing. Unlike CASSCF/CASPT2, the TD-DFT calculation did not find any MC transition for $[Ru(Cl)_2(CO)_2(iPr\text{-}DAB)]$ in the relevant energy domain. TD-DFT calculated population changes accompanying the lowest allowed electronic transition also point to a predominantly XLCT character with a small MLCT admixture. Inspection of Table 6 shows a huge decrease of electron density at the Cl atom(s), concurrent with a small population decrease on Ru and a large increase on Me-DAB. As in the case of the nonhalide complexes, TD-DFT predicts larger charge redistribution on excitation than CASSCF/CASPT2. This is manifested by the larger calculated population increase on Me-DAB.

In the far-UV region, TD-DFT underestimates the transition energies even more than in the visible region. The oscillator strengths and transition characters also differ from those calculated by CASSCF/CASPT2. In the case of $[Ru(Cl)(Me)(CO)_2(Me\text{-}DAB)]$, TD-DFT assigns the strongest transition as $4d_{xz}/p_{Cl} \rightarrow \pi^*_{DAB}$ (e^1A'), contrary to the $4d_{xy} \rightarrow \pi^*_{CO}$ (c^1A'') CASSCF/CASPT2 assignment. Nevertheless, both methods agree on the presence of a dense manifold of charge transfer states directed into π^*_{CO} orbitals in the far-UV region. For $[Ru(Cl)_2(CO)_2(Me\text{-}DAB)]$, TD-DFT found only forbidden transitions in this energy range.

To test whether the differences between the results obtained by the two approaches, CASSCF/CASPT2 and TD-DFT, lie in their very nature or if they are the consequence of technical computational details and particular approximations used, we have investigated also the effects of the CASSCF active space, the DFT functional, and the basis set. The use of a very large CASSCF active space (at the limit of the present computational possibilities) correlating 16 electrons in 15 orbitals for $[Ru(Cl)(Me)(CO)_2(Me\text{-}DAB)]$ revealed that the lowest allowed transition into the b^1A' state indeed has a partly mixed MLCT/XLCT character. The MLCT contribution is still predominant, accounting for ~55%, while XLCT character contributes 19%. The XLCT contribution arises from configurational interaction, instead of a $d_{Ru}-p_{Cl}$ orbital mixing, because the molecular orbitals involved are well localized either on the Ru atom or on the Cl atom, in the same way as those obtained by the 10e12a calculation, Figure 4. In addition, the 16e15a calculation found another transition of a reversed, XLCT/MLCT, character that occurs some 12 000 cm^{-1} higher in energy (at the CASSCF level). It has no counterpart in the 10e12a calculation whose results are reported in Table 5. This new state is composed of 15% MLCT and 59% XLCT characters. Unfortunately it has not been possible to perform the subsequent CASPT2 calculation on this zero order wave function for technical limitations. In the case of DFT calculations of $[Ru(Cl)(Me)(CO)_2(Me\text{-}DAB)]$, the use of: (i) a basis set identical to the one used for the CASSCF/CASPT2 calculations or (ii) a high-quality double-ζ basis set with diffuse functions on the Cl atom[37] does not modify significantly the TD-DFT results. The transition energy changes never exceed a few hundreds of wavenumbers. For instance, the a^1A'' and b^1A' states calculated at 14 440 cm^{-1} and 16 210 cm^{-1} (Table 5) are calculated at 14 650 cm^{-1} and 16 500 cm^{-1}, respectively, with the high-quality basis set. Only a moderate increase of transition energies is observed together with a slight increase of the MLCT character on adding diffuse functions to the Cl atom. This contrasts to the large influence of the basis set quality on the transition energies to the Rydberg states that was found in several cases.[38,39] Herein, this effect seems to be less important for valence states such as MLCT or XLCT. As far as the choice of the functional is concerned, B3LYP definitely gives the best transition energies. For instance, the use of B1LYP improves the results by 1000 cm^{-1} for the low lying forbidden transition to the a^1A'' state of $[Ru(Cl)(Me)-$

(37) Woon, D. E.; Dunning, T. H., Jr. *J. Chem. Phys.* **1993**, *98*, 1358.
(38) Tozer, D. J.; Amos, R. D.; Handy, N. C.; Roos, B. O.; Serrano-Andrés, L. *Mol. Phys.* **1999**, *97*, 859.
(39) Tozer, D. J.; Handy, N. C. *J. Chem. Phys.* **1998**, *109*, 10180.

$(CO)_2$(Me-DAB)], but the overall performance of this functional within the whole series of complexes is a bit worse than that of B3LYP. The transition energies calculated with the BP or BLYP functional are completely out of range, because they are some 7000 cm^{-1} lower than the experimental values. The same trends are observed for [Ru$(SnH_3)_2(CO)_2$(Me-DAB)], but in this case, the effect of the functional on the excitation energies seems to be less important than in the Cl-substituted complex. The underestimation of transition energies using the BLYP functional has also been observed on small systems.[39] The basis set and functional effects on the TD-DFT transition energies as well as the CASSCF active space effects will be discussed in detail elsewhere.[36]

The remarkable spectral difference observed upon replacing the SnH_3 ligands by Cl ligands in [Ru$(SnH_3)_2(CO)_2$(Me-DAB)] and [Ru(SnH_3)(Me)$(CO)_2$(Me-DAB)] is caused by reversing the order of the low-lying SBLCT and MLCT (or MLCT/XLCT) excited states. This has profound consequences not only on the absorption and emission spectra of the two classes of complexes but also on their photoreactivity. Theoretical investigations of the photochemical Ru−Sn and Ru−Me bond homolysis on the basis of excited-state potential energy curves are in progress.[18]

Conclusions

The UV−visible spectra of a series of [Ru(E)(E′)$(CO)_2$(α-diimine)] complexes has been investigated on the basis of theoretical and experimental analysis of the spectra of model and real molecules. The calculated absorption spectra have been obtained through two different theoretical approaches, namely the TD-DFT and the CASSCF/CASPT2 methods. The agreement between the two approaches is remarkably good for the [Ru$(SnH_3)_2(CO)_2$(Me-DAB)] and [Ru(SnH_3)(Me)$(CO)_2$(Me-DAB)] models. The calculated transitions account very well for the experimental spectra of [Ru$(SnPh_3)_2(CO)_2$(iPr-DAB)] and [Ru$(SnPh_3)$(Me)$(CO)_2$(iPr-DAB)]. The transition $\sigma_2 \rightarrow \pi^*_{DAB}$ (SBLCT) calculated around 20 000 cm^{-1} is responsible for the strong absorption observed in the visible spectral region for both complexes. In contrast, the CASSCF/CASPT2 and TD-DFT approaches lead to different descriptions of electronic transitions of the halide complexes [Ru(Cl)(Me)$(CO)_2$(Me-DAB)] and [Ru$(Cl)_2(CO)_2$(Me-DAB)] which are the model systems for the iPr-DAB substituted molecules. Even if the overall spectral assignments are qualitatively similar, an analysis of the Kohn−Sham orbitals and of changes in electron density distribution (i.e., Mulliken populations) upon excitation shows that the character of the low-lying excited states differs in both methods, apparently because of a different treatment of electron correlation. Indeed, whereas the lowest band observed in the visible region has been assigned to essentially pure MLCT by the CASSCF/CASPT2 approach, these electronic transitions are best described as mixed XLCT/MLCT by DFT, where XLCT stands for a Cl → DAB excitation. The TD-DFT method systematically underestimates transition energies in the halide complexes. This discrepancy is essentially invariant to changes in the CASSCF active space, the choice of a DFT functional, or the basis set used. Nevertheless, the main trend is well reproduced by both methods: substituting the SnH_3 ligands by Cl ligands in [Ru$(SnH_3)_2(CO)_2$(Me-DAB)] and [Ru(SnH_3)(Me)$(CO)_2$(Me-DAB)] causes the inversion of the order of the low-lying SBLCT and MLCT (XLCT/MLCT) excited states. This has profound consequences for both their spectroscopy and photoreactivity.

In all investigated cases, the CASSCF/CASPT2 and Kohn−Sham orbitals were calculated to have somewhat different characters and extents of delocalization. Even the bonding/antibonding character with respect to specific bonds may differ. The Kohn−Sham orbitals are generally more delocalized than the CASSCF/CASPT2 ones. Despite that, TD-DFT indicates that the lowest allowed electronic transitions are accompanied by larger electron density redistribution than that calculated by CASSCF/CASPT2. These findings clearly show that the common qualitative arguments based on one-electron molecular orbitals are of a limited value and have to be used with a great care. The present results illustrate the difficulty for the DFT approach in describing excited states in systems containing bonding between a halide and a low-valent metal atom. In this context, development of functionals based on a multiconfigurational scheme will be very important for future investigations of spectroscopic properties in transition metal complexes.

Acknowledgment. This work has been undertaken as a part of the European collaborative COST project (D14/0001/99). We thank the Departement de Chimie of the CNRS for specific COST financial support. M.T. thanks the Centre National des Œuvres Universitaires et Scolaires and the Tunisian government. The CASSCF/CASPT2 calculations have been carried out either at the IDRIS (Orsay, France) through a grant of computer time from the Conseil Scientifique or at the LCQS (Strasbourg, France).

JA010782B